Geology, Geophysics & Environment 2023, vol. 49 (2): 157–173

Tectonic strain in salt rock mass based on measurements

Zbigniew Szczerbowski[1], Zbigniew Niedbalski[2], Łukasz Bednarek[3]

[1] *AGH University of Krakow, Faculty of Geo-Data Science, Geodesy, and Environmental Engineering, Krakow, Poland, e-mail: szczerbo@agh.edu.pl, ORCID ID: 0000-0002-2398-559X*
[2] *AGH University of Krakow, Faculty of Civil Engineering and Resource Management, Krakow, Poland, e-mail: niedzbig@agh.edu.pl (corresponding author), ORCID ID: 0000-0003-0497-0162*
[3] *AGH University of Krakow, Faculty of Civil Engineering and Resource Management, Krakow, Poland, e-mail: bednarek@agh.edu.pl, ORCID ID: 0000-0002-8239-5864*

Received: 10 August 2022; accepted: 20 February 2023; first published online: 13 March 2023

Abstract: The measurement method with the application of an extensometer for the detection of the manifestation of tectonic strain is presented in this paper. The instrument is operated in underground construction for engineering purposes, and the authors applied it in a deeply placed underground old mine gallery in the Bochnia Salt Mine, just at the tectonic boundary of the Outer Carpathians which is commonly considered to be a tectonically active zone. The presented study is characterized by two basic features. The first is the placement of the measurements deep in an old mine which is an environment free of atmospheric factors disturbing the detection of a tectonic signal. The second is a combination of routine measurements carried out for engineering purposes and research measurements enabling the extension of the observation of displacements in the space outside underground workings, inside the rock mass that has been penetrated by extensometer probes. The extensometric measurements have been made using three 7-meter long sections. The results showed the differentiation in the displacement rates of points placed in the side walls: in the southern profile, the annual displacements are approximately 1.5 mm and in the northern one – approximately 1 mm. The combined result corresponds to the amount of the annual convergence value which has been determined by the classical surveys in the excavation where extensometric measurements have been made. What is more, the ongoing displacements in the southern side wall involve the entire part of the rock mass which is penetrated by an extensometric probe, but the displacements in the northern side are only observed in the first 2 m of the penetrated part of the rock mass. This differentiation is interpreted by the authors as being the result of tectonic strain acting from the south exerted by the Carpathians.

Keywords: rock salt, tectonic stress, convergence, rock strain, extensometers, numerical modeling

INTRODUCTION

The Bochnia Salt Mine has been operating as a mine for nearly 800 years and for almost forty years as a museum inscribed on the UNESCO World Heritage List (Garlicki 2008, 2013, Wiewiórka et al. 2009). Due to its unique historical and natural values, the Bochnia Salt Mine is under constant maintenance and underground safety works are still in progress. Fundamental in this activity is the geodetic monitoring of the underground excavations for the maintenance and continuous protection of the underground historical excavations. It also helps to safeguard the development of the town of Bochnia (Wiewiórka et al. 2009, Szczerbowski 2020). Any losses in the stability of the old mine workings could have led to a construction disaster on the ground level in the form of sinkholes (d'Obyrn et al. 2013, Malinowska et al. 2019, Stoeckl et al. 2020).

This monitoring provides the detection of upward transitions of deformation from underground which may pass through the rock mass overlying the salt deposit and even reaching

the surface (Kratzsch 1986, Szostak-Chrzanowski et al. 2005, Szwedzicki 2018). Surveying methods are used to assess the phenomena occurring inside the rock mass and to note any expected changes which may occur on the terrain surface, as well as to study any terrestrial deformations (Knauss & Steinborn 1980, Kortas 2004, Bieniasz & Wojnar 2007, Szczerbowski et al. 2016). The main result of the measurements is then presented as displacements of control points expressing rock mass movements of either the entire chamber or its individual elements, and also the differentiation of this process which in individual cases provides evidence of geometric deformations (convergences, strains).

The presented paper is a continuation of research carried out with the use of a sonic probe extensometer (Szczerbowski & Niedbalski 2021) in the Bochnia Salt Mine. Additional background data not dealt with in this paper can be found in a previous paper.

The area under study is located at the contact zone of two large tectonic units: the Carpathian Foredeep Basin and the Outer Carpathians. This makes it an ideal place for the investigation of the contemporary tectonic activity of the Carpathian orogen (Fig. 1).

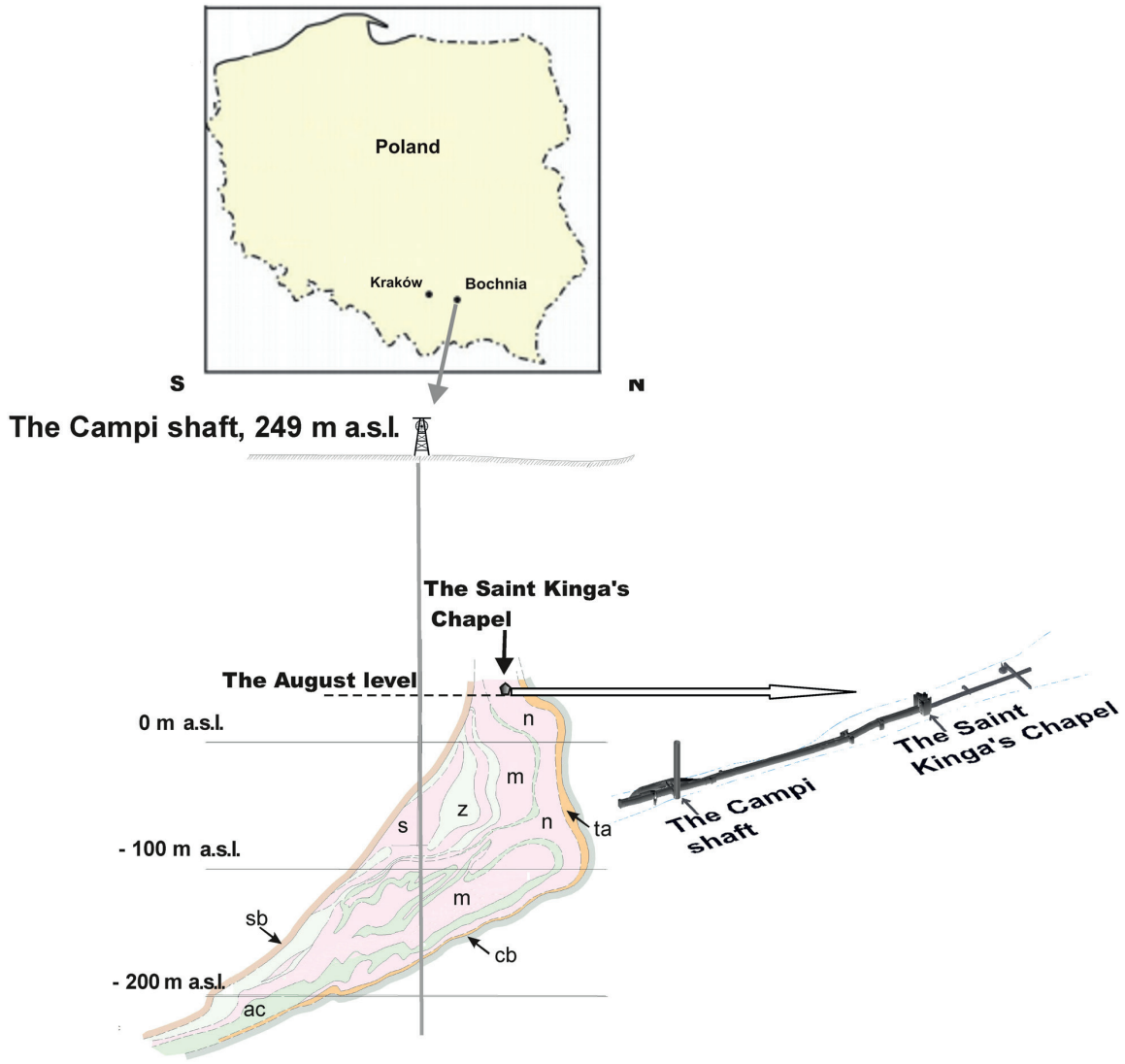

Fig. 1. *Location of the Bochnia salt deposit with the test field at the Saint Kinga's Chapel and simplified geological cross section (based on Poborski 1952, Wiewiórka et al. 2009, modified): cb – Chodenice beds, ta – top anhydrite, n – northern salts, ac – anhydritic claystones, m – middle salts, z – upper zuber, s – southern salts, sb – Skawina beds*

The rock mass deformations observed underground by geological methods (Toboła & Bezkorowajny 2006) and determined by geodetic measurements (Szczerbowski et al. 2016) were interpreted by the authors of former studies as manifestations of recent neotectonic activity. This research study focuses on deformation in the intact rock salt surrounding the gallery, and rock salt geometrical changes (convergence).

This paper provides a contribution to the discussion on the manifestation of neotectonic processes in salt mines in Wieliczka and Bochnia and which has been going on for a number of years (Poborski 1982, Toboła & Bezkorowajny 2006, Szczerbowski et al. 2016, Burliga et al. 2018).

THE MEASUREMENTS

Displacement is the basic parameter depicting the deformation process that may be determined by surveying methods. In the rock salt mass in the Bochnia mine, both horizontal and vertical components of the displacement vectors are similar, which is curious when compared with other types of rock mass (Kortas 2004). The surveying measurements provide data that can determine convergence applied in the deformation control and periodic safety assessments in Bochnia. Convergence is the closure of the workings (chambers, passages etc.). Convergence refers to the negative increment in the distance between the walls of the excavation, which results in the expression of convergence in linear units, e.g. in millimeters.

The finite closure process in the salt rock mass takes place over a very long time (hundreds of years), which results from the rheological properties of the salt (Jeremic 1994, Kortas 2004). An important feature of salt rock mass is the maintenance of the coherence and continuity of deformation over time, but any exceeding of the strength limit causes the loss of rock mass cohesion and leads to collapses.

Strain is defined as relative displacement. Depending on the understanding of the term "relative displacement", there are different approaches to determining this quantity. Apart from small strain, the common types of strain measure (engineering strain, Cauchy strain, logarithmic strain) may be reduced to the engineering strain, which is expressed as the ratio of the total deformation to the initial dimension of the material body on which forces are applied. This type of strain measure is commonly applied in surveying but in Bochnia it is of secondary importance in the planning of protection works.

There are two basic surveying measurement methods which are applied in the case of the underground monitoring in Bochnia (Kortas 2004, Bieniasz & Wojnar 2007):

1) leveling, which provides data determining the vertical displacements like subsidence or uplift (which is quite rare); on the base of multiple measurements vertical convergence and vertical strain are estimated;
2) distance measurements (extensometric), which provide data determining the rate of the horizontal or vertical rock mass displacement (compactions and extension) and the rock mass horizontal or vertical strain.

A combination of the methods provides data on volume convergence. The scheme presented in Figure 2 shows the relation between the methods, obtained results and quantities. Besides, there are additional methods applied underground as electromagnetic extensometer measurements or laser scanning measurements. In terrestrial monitoring GNSS, leveling and tachymetric measurements are used for assessing the determination displacements of control points or benchmarks.

The chapel is well monitored due to a number of control points comprising the surveying infrastructure. The results are derived from deformation measurements and are based on geodetic control points. Figure 3 shows the layout of the monitoring network and the location of control points creating a spatial network in the Saint Kinga's Chapel. Points are placed on the walls, on the floor and on the roof of the chapel. The total number of the control points used in the horizontal distance (convergence) measurements is about 60 and they form about 30 baselines, which are applied for the determination of the horizontal convergence of the chapel and strain. Additionally, there are about 20 control points (benchmarks) used in leveling. The area of the chapel is about 340 m^2 and its perimeter amounts to 103 m.

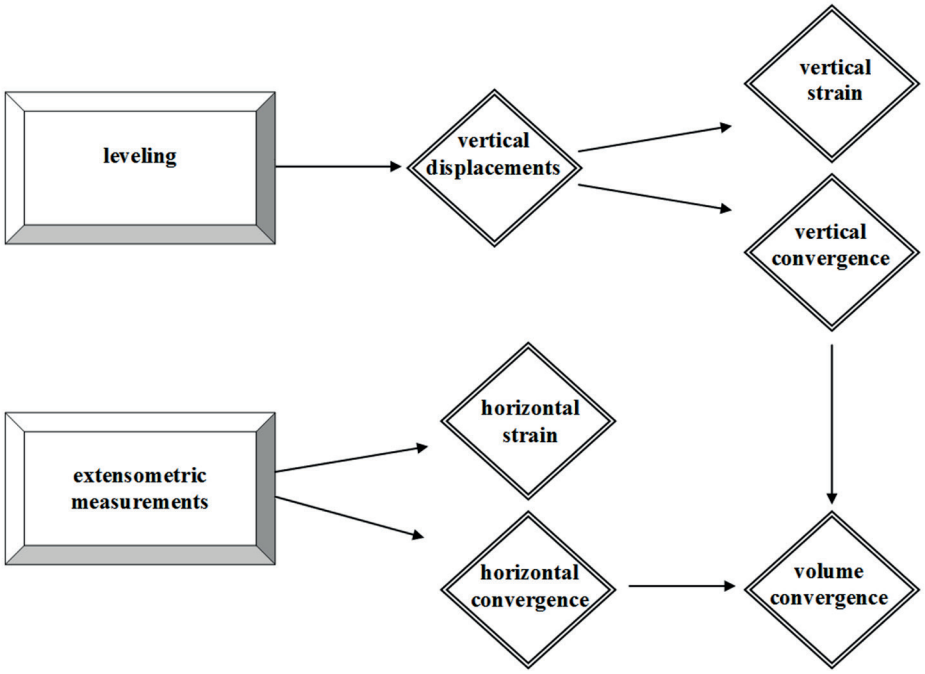

Fig. 2. *Scheme illustrating deformation parameters obtained by measurement methods applied in underground deformation monitoring in the Bochnia Salt Mine*

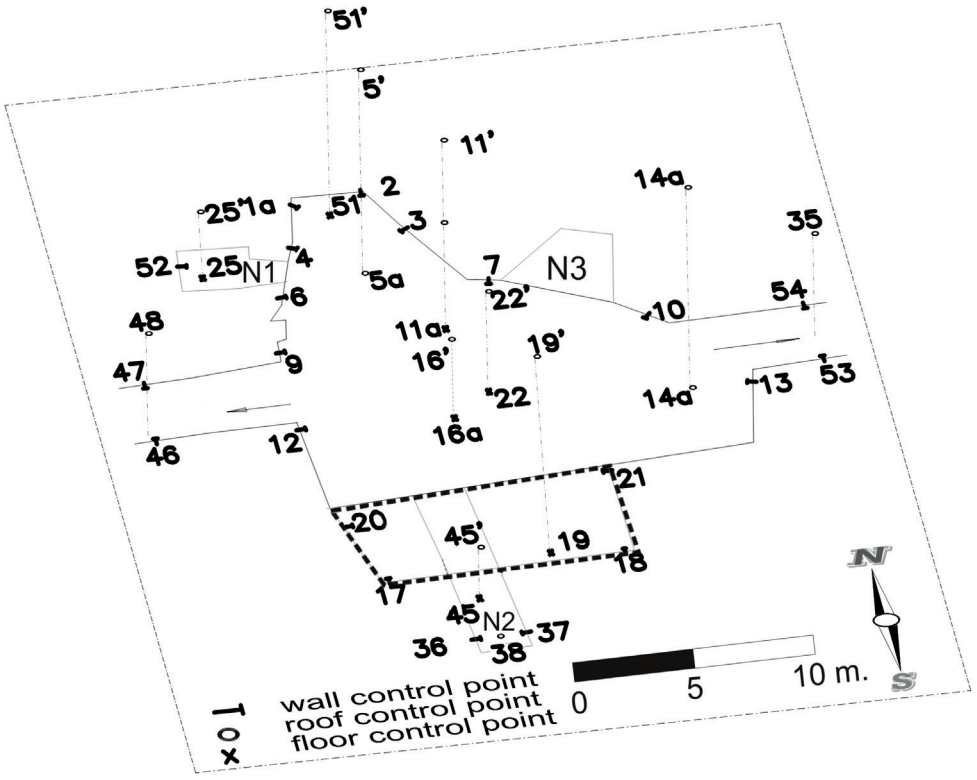

Fig. 3. *The Saint Kinga's Chapel. The spatial distribution of the selected control points and the baselines. The area with dashed borders is the choir (the back side of the main part of the chapel) and N1, N2, N3 are the niches*

Considering the length and the orientation, five types of baselines can be distinguished:

1) N-S oriented long baselines (over 20 m long),
2) N-S oriented short baselines (about 3 m long), they are placed in the roadway, close to the entrance to the chapel,
3) E-W oriented short baselines (about 3 m long), they are placed in the niches of the chapel,
4) E-W oriented long baselines (8–17 m long),
5) one oblique, the ESE-WNW oriented baseline (18.5 m long).

The measurements have been performed at many benchmarks for over 20 years. Due to the number of bases increasing in time, we used a 10 year measurement period. The leveling and length measurements have an accuracy of approx. 1 mm.

Table 1 presents deformations expressed in displacement, convergence, and strain rates. Very short (about 1 m) baselines used for observations in the niches were rejected as not representative in the further analysis.

Table 1

Compilation of deformation parameters calculated on the base of measurements of selected control points and baseline involved in measurements in the Saint Kinga's Chapel in the Bochnia Salt Mine in the 2012–2021 year period. Downward displacement and distance reduction are expressed by negative values

Control points	**Displacement [m/yr]**		
5	−0.007		
5'	−0.013		
11	−0.006		
11'	−0.014		
14	−0.007		
16	−0.006		
16'	−0.014		
19	−0.01		
19'	−0.015		
22	−0.01		
22'	−0.014		
25	−0.008		
25'	−0.011		
35	−0.014		
38	−0.013		
45	−0.011		
45'	−0.013		
48	−0.018		
51	−0.008		
51'	−0.011		
Vertical baselines	**Baseline length [m]**	**Convergence [mm/yr]**	**Strain rate [mm/m/yr]**
5–5'	5.5	−5.7	−1.0
11–11'	5.5	−7.7	−1.4
14–14'	2.4	−8.6	−3.5
16–16'	5.2	−8.5	−1.6
19–19'	3.3	−4.4	−1.35
22–22'	3.2	−4.8	−1.5
25–25'	2.0	−3.4	−1.7
45–45'	1.9	−1.2	−0.6
51–51'	5.4	−3.1	−0.6

Table 1 *cont.*

Horizontal baselines	Baseline length [m]	Convergence [mm/yr]	Strain rate [mm/m/yr]
52–10 (oblique baseline)	18.5	1.0	0.06
1a–17 (baseline S-N)	25.1	–7.4	–0.3
2–18 (baseline S-N)	25.4	–8.6	–0.3
46–47 (baseline S-N)	3.3	–12.4	–3.7
55–56 (baseline S-N)	2.4	–11.4	–4.8
53–54 (baseline S-N)	2.4	–7.4	–3.2
3–4 (baseline W-E)	3.7	–3.3	–0.9
6–7 (baseline W-E)	8.3	–1.8	–0.2
9–10 (baseline W-E)	14.7	–2.5	–0.2
12–13 (baseline W-E)	17.5	–5.6	–0.3
20–21 (baseline W-E)	8.8	–3.5	–0.4

One of the noticeable features of the results is the similarity of horizontal compression strain values determined for the baselines within the space of the chapel (52–10, 1a–17, 2–18, 3–4, 6–7, 9–10, 12–13, 20–21). The values determined for the baselines located in the western roadway at the entrance to the chapel (46–47) are much higher. The baselines in that place, depending on the level of their baseline position, indicate strain rates of from –3.0 to –5.0 mm/m/yr, which is much higher than the average value of the strain rates determined inside the chapel (from –0.2 to –0.9 mm/m/yr). On the other hand, however, the rates determined for the three baselines in the roadway at the eastern entrance (53–54) are –3.2 mm/m/yr, so they are smaller than at the western entrance, but clearly higher than those found on the inside of the chapel as well. This differentiation of the values of the strain within this short distance between baselines is surprising.

Figure 4 presents the combined distributions of the deformation parameters: vertical displacements of the floor benchmarks and vectors of horizontal displacements are modeled on the base of the horizontal convergence. The approximate model of the horizontal displacements is based on the assumption that the points of the particular baseline have the same amount of displacement values, but their directions are opposite. Then, having the values of horizontal displacements at these points, interpolation was carried out using the kriging method in order to obtain the distribution of displacement values at points where no measurements were made. The arrows indicate the modeled horizontal displacement vectors. This method was also applied for the determination of the vertical displacements.

The values of baseline length, horizontal convergence, and horizontal strain determined for the space of the chapel are to some extent interrelated. There are two population groups of the data: the first is a small representation of baselines with quite a wide range of strain rate values (from about –4.5 to –2.5 mm/m/yr) and convergence values (ranged from –14 to –6 mm/yr). Most of the data are within a narrow range of strain rate (values from –0.9 to –0.1 mm/m/yr) and the convergence values correspond to lengths of baseline. The general examination of the distribution of points in the space defined by the system of axes representing the deformation parameters (strain, convergence) and the lengths of the corresponding baselines allows us to determine the presence of two data populations. The first refers to points representing bases located in the roadways. In this case, a large dispersion of the corresponding deformation values is visible. The second group, more ordered in terms of the geometry of their distribution, represents the bases located inside the chapel, and their convergence and strain values are found to be quite regularly spaced.

The distributions of strains and convergence values in respect to the baseline lengths are presented in Figure 5 and confirm the direct relationship between the values of baseline length and convergence.

There are two plots presented here, and the first demonstrates this relationship. This dependency seems to be linear, and this relationship does not exist between length and strain (Fig. 5).

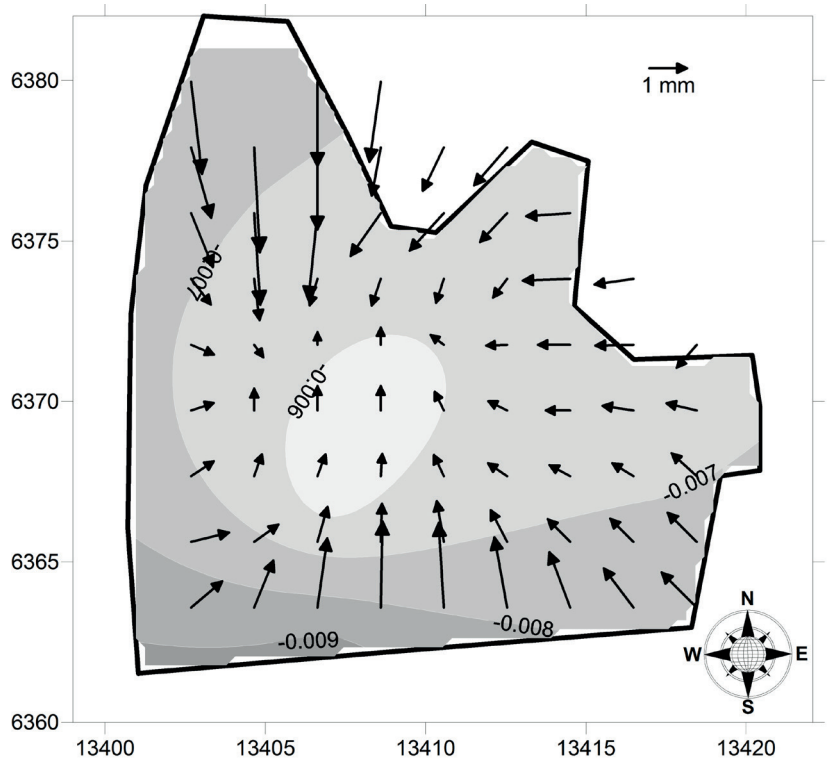

Fig. 4. *The Saint Kinga's Chapel vertical displacements of the floor benchmarks [mm/yr] outlined by isolines and vectors of horizontal displacements modeled on the base of the horizontal convergence (outlined by arrows with length representing displacement). The local coordinate system [m]*

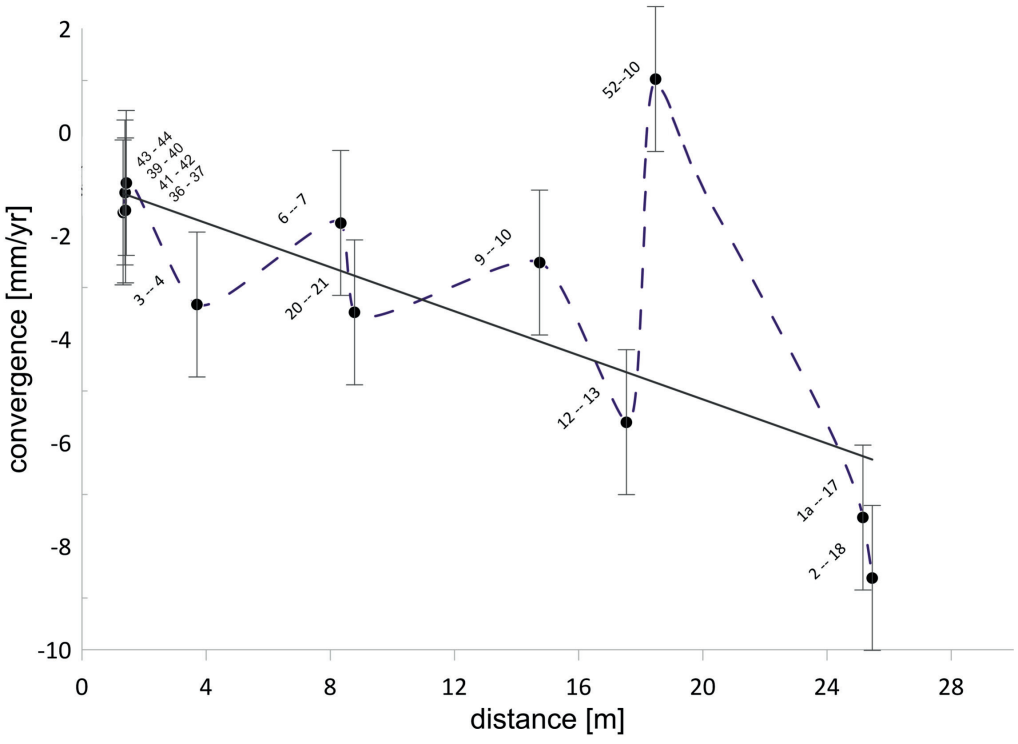

Fig. 5. *Convergence values versus baseline length with error bars, a comparison of the data based on convergence measurements in the Saint Kinga's Chapel with suggested linear trend (continuous line)*

There are some more observations that may arise after analyzing the distributions of the strains and convergences depending on the length of the bases. All of the convergence values determined for the baselines located in the chapel (together with short ones located in the niches) are presented in Figure 5.

Although there is a noticeable regularity in the relationship between the length of the baselines and the convergence values for both long and short baselines, one can notice an outlier value in the plot (18.5 m at *x*-axis). This data point differs significantly from other strain values determined for the baseline of the ESE-WNW orientation and it extends from the right wall of the chapel to the niche, which isn't strictly associated with the nave of the chapel.

The next plot on the same figure presents the distribution showing the relationship between the strain rate values and baseline lengths. There are three main groups of the data population representing the baselines placed in (Fig. 6):

A. the main body of the chapel,
B. the niche in the southern part of the chapel,
C. the roadway at the western and the eastern entrances to the chapel.

The first group demonstrates the constant strain rate values independently of the lengths of the baseline with the average value amounts to −0.33 mm/m/yr. Thus the nave of the chapel demonstrates a stable horizontal strain rate and provides an illustration of the constant effect of forces acting around the excavation.

The other data which are characterized by noticeable diversity represent strains as if they were the result of a different stress regime. So, the second group (B) demonstrates a noticeable dispersion of strain values at similar lengths of the baselines – all of them are located in the niche in the southern part of the chapel (and in a very short tunnel connecting the main part of the chapel with this niche). The average strain value of this group amounts to about –1 mm/m/yr. The last group (C) shows the presence of a significant distribution discrepancy ranging from –2.3 to –4.4 mm/m/yr. So, it may be seen that the values of the vertical strain are 3 times higher than the horizontal ones (with some exceptions) within the nave of the chapel and they correspond to the horizontal strain values observed in the roadway (Table 1). However, the values of the vertical strains are more even, even though the differentiation of the vertical baseline length is higher.

Summarizing the abovementioned remarks, it can be concluded that within the analyzed space the reaction of the rock mass flow due is quite proportional to the free space in a particular direction. The lengths of the horizontal baselines extended in particular directions are limited by the presence of the side walls of the irregularly shaped chapel and they control and affect the values of the convergence to keep the strain values constant. The horizontal strain values are in an order of magnitude smaller than the vertical ones.

Similar results can be inferred from the convergence measurements for the baselines placed in the roadways. However, the measurements in the passages at the western and the eastern entrances to the chapel provide a different displacement characteristic. At the western entrance there are two horizontal baselines (55–56 and 46–47) and one roof benchmark (48). The distance measurements of the baselines, where the observed convergence has been an average –12 mm/yr since 1998, the strain rate value amounts to an average –4.3 mm/m/yr. The displacements, convergence and strain are outlined on Figure 7 as follows: the yellow arrows with a continuous line represent displacement vectors, the white lines represent the baselines of the convergence measurements, the red arrows represent the vertical strain and the blue one a horizontal strain. The values marked in a white color show the values of convergence [mm/yr], the horizontal strain is in a blue color [mm/m/yr], the vertical strain is in a red color [mm/m/yr] and the vertical displacement rates are in a yellow color [mm/yr].

The value of the vertical convergence and strain can be estimated on the basis of both the determined the vertical displacements of the roof benchmark (dH_{roof}) which is located just above the baselines and the displacements of the floor benchmark (dH_{floor}) which is located nearby. The following equation expresses the rate of the strain of the vertical baseline, and the dividend expresses its convergence:

$$\frac{dH_{roof} - dH_{floor}}{H_{roof} - H_{floor}},$$

where $H_{roof} - H_{floor}$ is the difference between the heights of the roof benchmark (H_{roof}) and the floor (H_{floor}) benchmark.

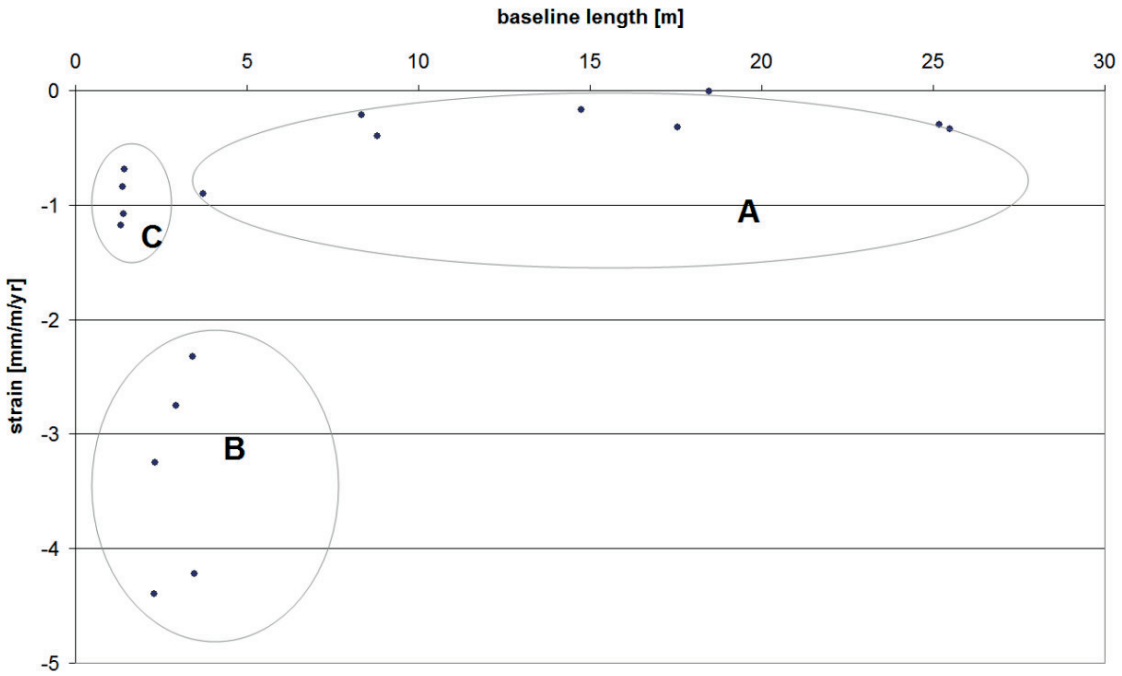

Fig. 6. *The relationship between strain and baseline length, a comparison of the data based on convergence measurements in the Saint Kinga's Chapel*

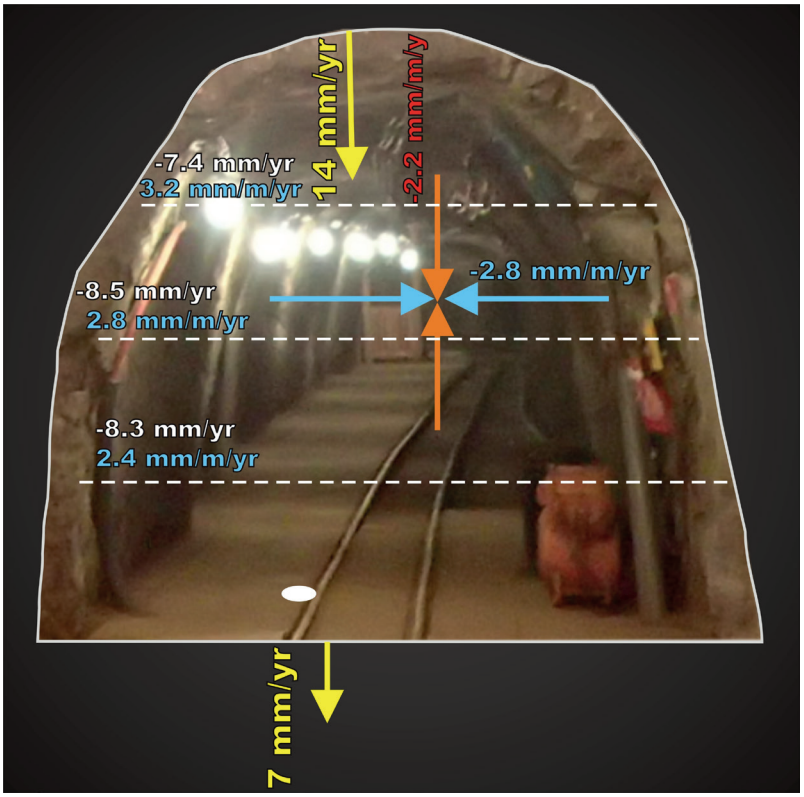

Fig. 7. *The deformation parameters obtained on the basis of mine surveying measurements in the test field at the entrance to the Saint Kinga's Chapel*

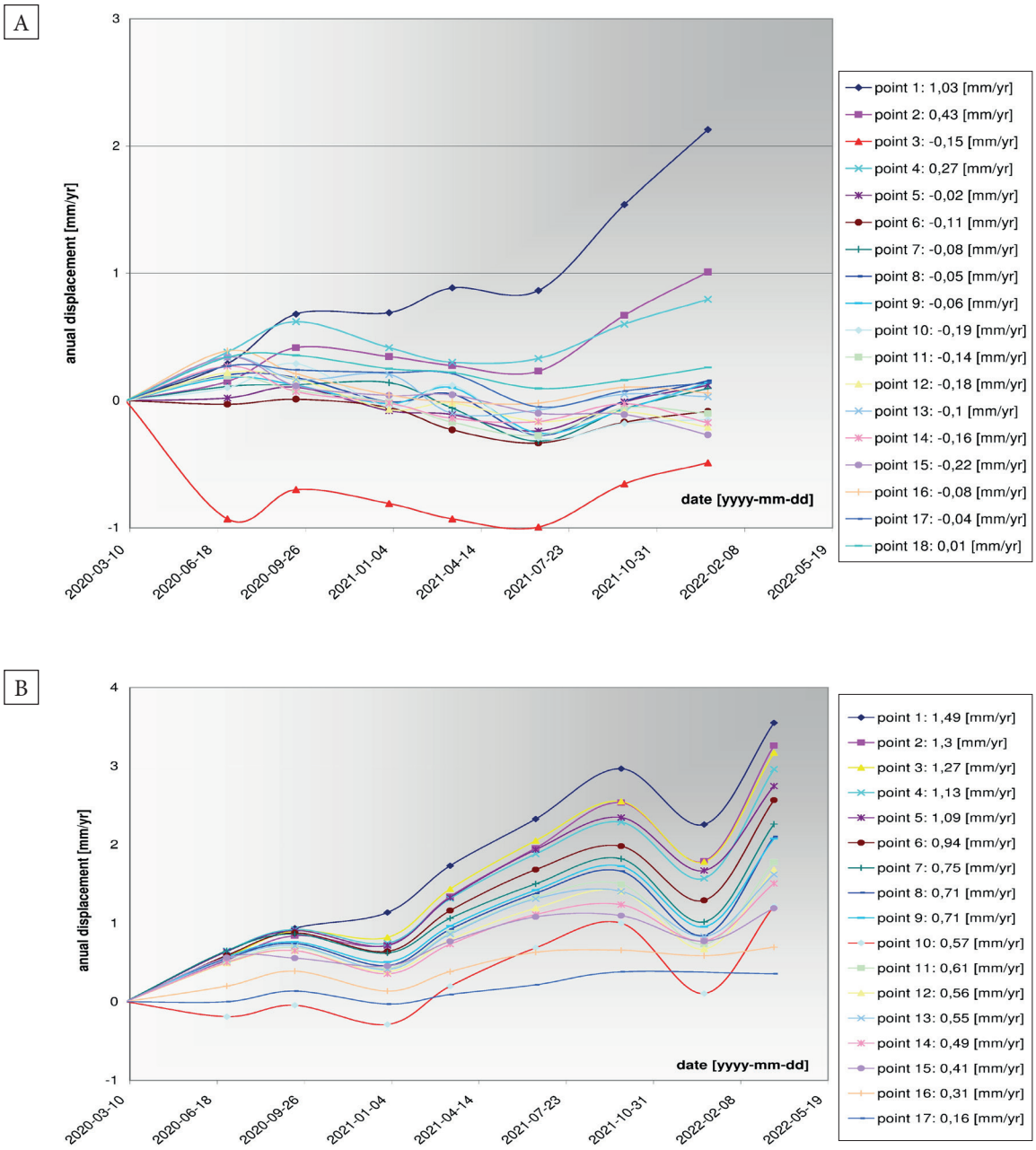

Fig. 8. *Total displacements of points between March 2020 and March 2022 in the following measurement baselines: A) N (northern side wall); B) S (southern side wall) on the right-hand side graph*

This is an approximate approach because there are no direct measurements from the floor to the roof. By this method of measurement, the estimated vertical convergence at the western entrance to the chapel was found to amount to 12 mm and the strain value to amount to 4.1 mm/m/yr.

More valuable are the observations at the eastern entrance to the chapel where extensometer measurements have been already carried out for several years. The principle of the measurement and use of a magnetic extensometer are discussed in a previously mentioned paper (Szczerbowski & Niedbalski 2021). Apart from where previous results were often disturbed by unexplored source disturbances measured over a period of 2 years, there is a clear trend in the displacements of all the points with a rare deviations in individual cases.

Three boreholes were drilled in a profile of the roadway at the eastern entrance to the chapel and each of them consisted of a protective tube (7.5 m long and 45 mm in diameter) with magnetic anchors (Szczerbowski & Niedbalski 2021). They were placed along the whole length of the tube, and were placed at a distance of about 30 cm from each other. Such boreholes make an investigation site for the monitoring of the deformation propagation in the rock salt around the excavation: in the southern side wall (S base), in the roof (ST base) and in the northern side wall (N base).

Between March 2020 and March 2022, we were able to collect the results which are presented in Figure 8.

As can be seen, the characteristics of the displacements in the southern and northern profiles are different. This difference is more evident in the form of the plots outlining the distribution of the displacement rates of the points in the S and the N profiles (Fig. 9). The compilation shows an asymmetry in the distribution of the displacements between both sides of the gallery. While the values quickly decrease on the northern side and completely disappear within a short distance, on the southern side an incessant increase in displacements towards the gallery can be observed, and the rates of displacement clearly increases as one approaches the side wall.

The distribution is asymmetric and illustrates the completely different action of forces causing the displacement of points from the S and N sides. A linear increase of displacements from the S side towards the roadway is clearly visible. In turn, on the opposite northern side, an increasingly rapid slowdown of point displacements is characteristic, and they are only observed at a distance of up to 2 m from the excavation. The authors analyzed these results and related them to the mining situation in this area to better understand this specific distribution of the displacements.

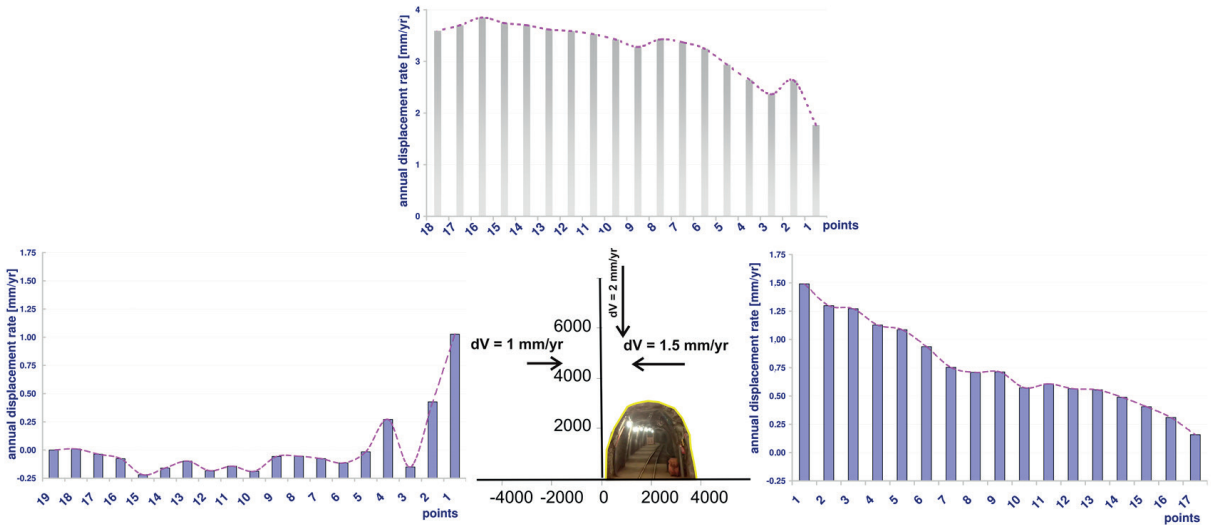

Fig. 9. *Distribution of the annual displacement rates of the points in the ST (above), the S (on the right) and the N profiles (on the left)*

THE MODEL OF DEFORMATION PROPAGATION

The next stage in the study was a numerical analysis for the determination of a theoretical deformation model, particularly a model of displacements.

The measurement results were related to the values obtained from the numerical modeling simulation, where the displacement field was determined in a homogeneous rock mass layer. The geomechanical parameters of rocks building the Miocene formation and salt deposit at

the Carpathians front were adopted from literature (Chmura & Lasoń 2005, Cała et al. 2009, Małkowski et al. 2019) and show in Table 2. Calculations were made to determine the stress distribution, fracture zones, and the size of the displacements around a theoretical gallery at the eastern entrance to the Chapel (the August with the test field). The calculations were made in the RS2 program using the Coulomb–Mohr strength criterion and the plastic model with the associated flow law – the dilatancy equals zero. RS2 is a 2D finite element program for geotechnical structures used in construction and mining. Applicable to rock, RS2 is a general purpose finite element analysis program including tunnel and support design.

The model's dimensions of 40 m × 40 m. The model mesh consisted of 1,611 elements and 3,353 nodes (Fig. 10). The layer system was adopted from geological cross-sections of the salt deposit and the surrounding rock layers (Andreyeva-Grigorovich et al. 2003, Wiewiórka et al. 2008, d'Obyrn & Hydzik-Wiśniewska 2013, Puławska et al. 2021a, 2021b). Ground surface elevation was at the depth of 150 m. The shape of the excavation was prepared on the basis of measurements made using a laser rangefinder. The height of the excavation at the highest point was 3.40 m, while the width at the floor was 3.87 m.

The results of the calculations show that the main stress σ_1 has the highest values, it is about 21 MPa, on the contour of the excavation at the most sensitive points in this respect. The concentration of stress is also noticeable in the roof of the excavation, but they are smaller.

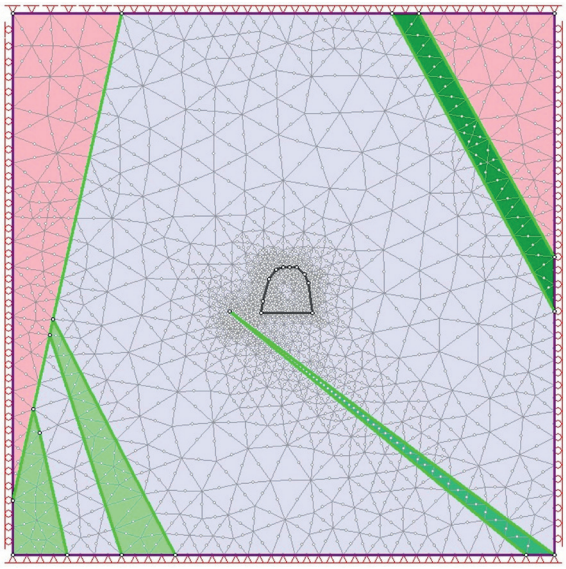

Fig. 10. *The assumed model of geological strata*

Figure 11 shows distribution of the main stress around the excavation.

The salt rock mass modeled in this way, despite not using the casing in the excavation, showed slight displacements. The displacements are particularly visible at the bottom of the excavation and amounted to 0.0134 m (Fig. 12). When analyzing the displacement map, it can be concluded that it is not symmetrical. This is especially discernible when interpreting displacements around the sides.

Using the obtained map of total displacements, lines were marked on it (Fig. 13), which correspond schematically with the boreholes in which measurements are made.

Table 2
Rock layer properties used in the numerical calculations

Lithology	Color on map	Unit weight [MN/m^3]	Poisson ratio [–]	Young modulus [MPa]	Tensile strength [MPa]	Friction angle [°]	Cohesion [MPa]
Northern and southern border claystones	pink	0.021	0.35	397	0.075	7.0	0.075
Lower, middle and upper barren formations	green	0.027	0.25	986	0.950	19.1	0.950
Northern and middle rock salt	light blue	0.021	0.28	1,100	2.500	57.0	3.900

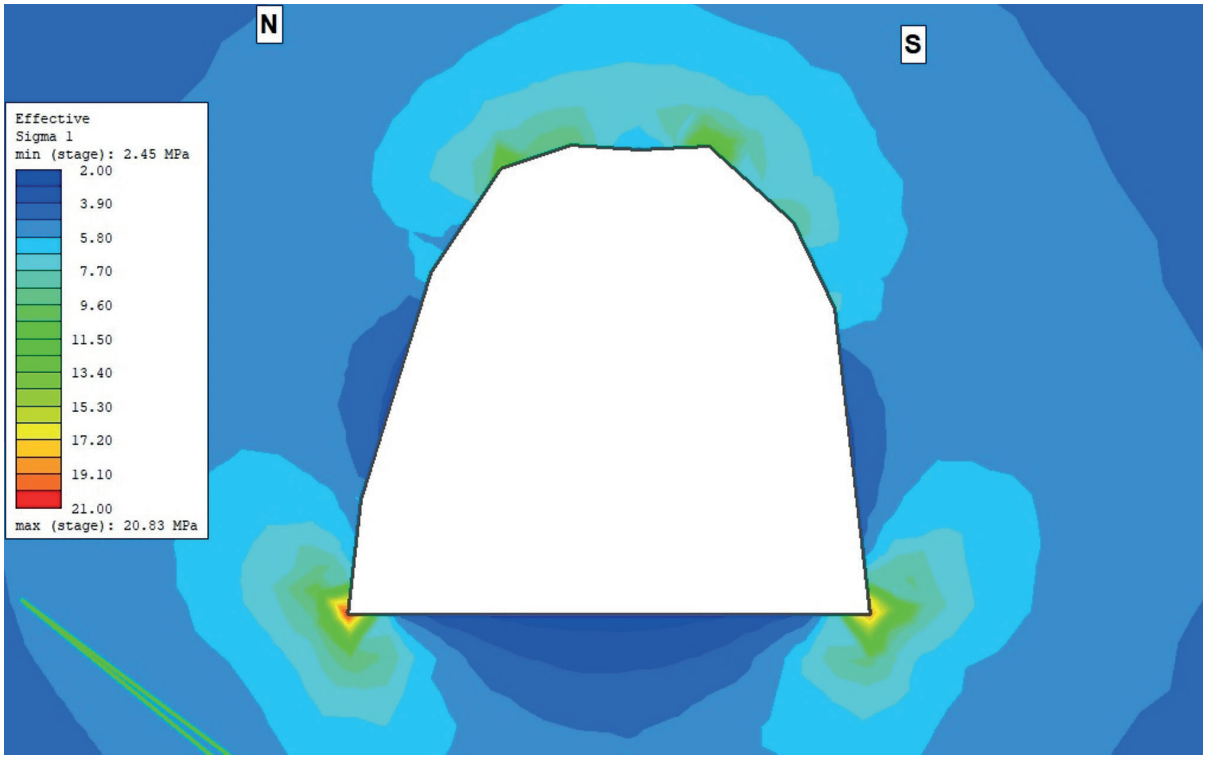

Fig. 11. *Distribution of main stress around the excavation*

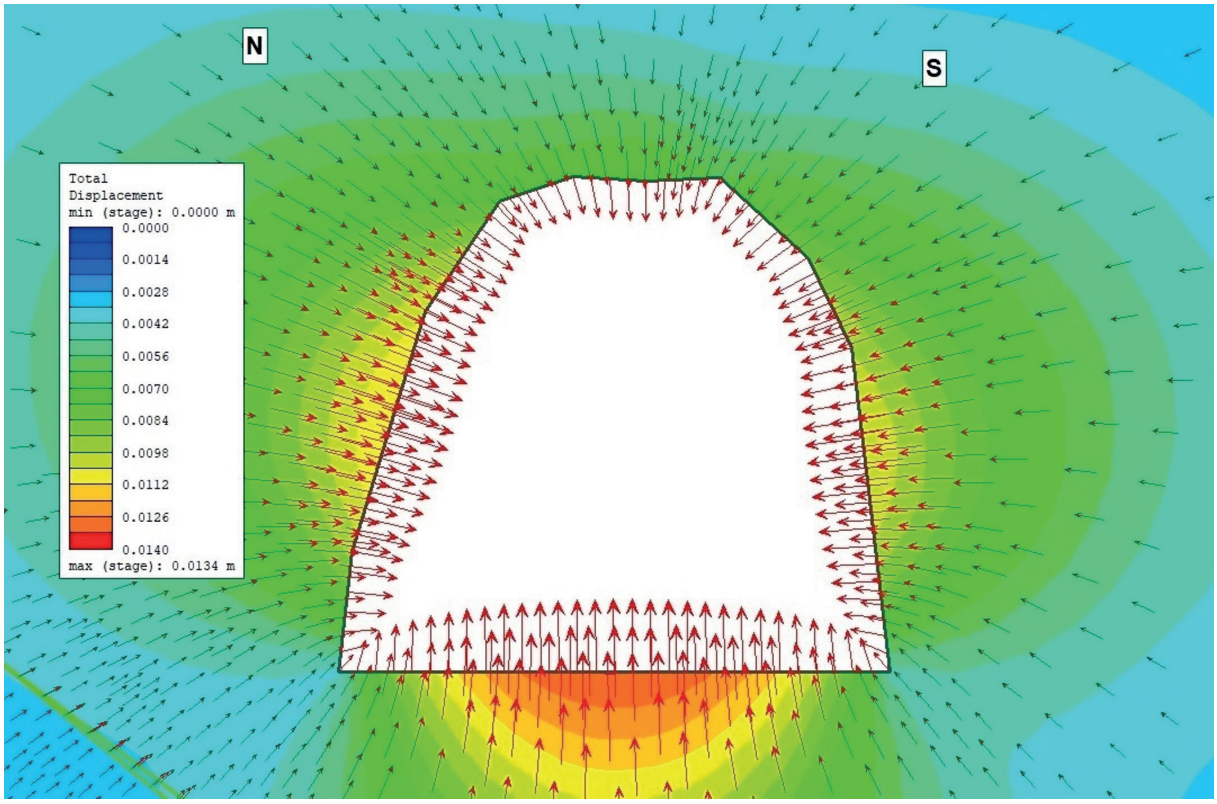

Fig. 12. *Distribution of total displacements around the excavation*

The modeled distribution of the displacements is quite regular and there are two main distinctive features:

1) quality: the symmetric pattern with the concentration of the displacements in the floor;
2) quite small values of the displacements determined for the total time interval of the measurements; in fact, they nearly amount to the annual rates determined by the measurements.

The characteristics suggest the occurrence of additional force (or forces) which play a dominant role in the process of the closure of the excavation. This theoretical model almost contrasts with the measurement results, where the lack of symmetry of the distribution is particularly visible. The asymmetry determined in the measurements is difficult to explain with the influence of other excavations. The only explanation is the presence of a tectonic force which is seen to be pressing from the south, and which is outlined in Figure 14. It presents the forces acting around the roadway and those results in deformations (displacement, convergence, strain).

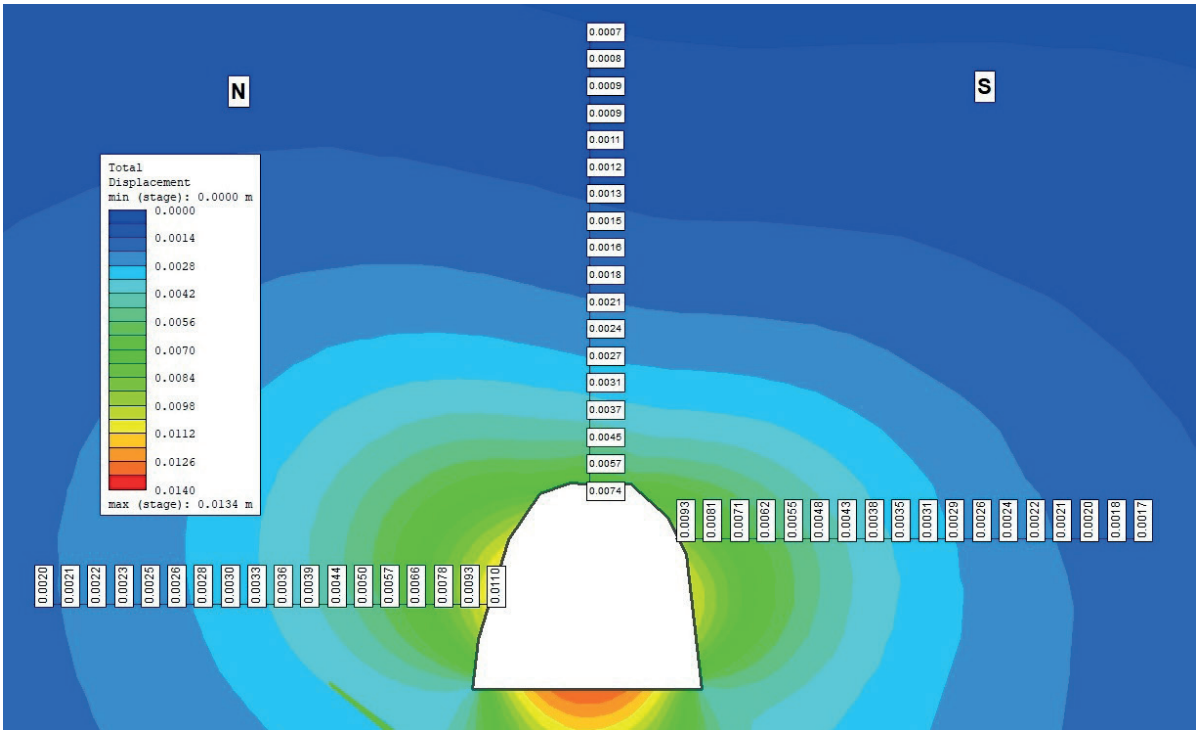

Fig. 13. *Theoretical total displacements of the points derived from the numerical analysis [m]*

Fig. 14. *The distribution of modeled displacement vectors determined on the basis of the measurements: the white arrows are displacement vectors whose rates were determined by the extensometric measurements, the yellow arrows are displacement vectors resulting from the process of convergence, the cyan arrows are displacement vectors resulting from the tectonic push*

Assuming that tectonic pressure is causing the movement of rock salt masses toward to the center of the excavation, tectonic forces acting from the south are causing the increase of the displacement values at the southern side wall but their decrease at the northern side wall (the vectors are in the opposite direction). So, at the southern wall and at the northern side wall we can observe the following effect of displacement driven by tectonics:

$\overrightarrow{v_S}+\overrightarrow{v_T}=\overrightarrow{v_{ST}}$ and $\overrightarrow{v_N}+\overrightarrow{v_T}=\overrightarrow{v_{NT}}$,

and it is assumed that the convergence process (as shown in the modeling presented above) affects the southern and northern side walls in the same way. Hence:

$\overrightarrow{v_S}=-\overrightarrow{v_N}$,

where:

- $\overrightarrow{v_S}$ – displacement vector resulting from rock mass movements stemming from the process of convergence and representing the southern side wall movements,
- $\overrightarrow{v_T}$ – displacement vector resulting from tectonic push,
- $\overrightarrow{v_{ST}}$ – displacement vector representing the southern side wall displacements and which result from rock mass movements caused by the process of convergence and tectonic push,
- $\overrightarrow{v_N}$ – displacement vector resulting from rock mass movements stemming from the process of convergence and representing the northern side wall movements,
- $\overrightarrow{v_{NT}}$ – displacement vector representing the northern side wall displacements and which result from rock mass movements caused by the process of convergence and tectonic push.

The displacement vectors around the excavation were determined on the basis of the measurements. On the northern side, as mentioned earlier, the annual rated amounted to about 1 mm/yr and at the southern one to about 1.5 mm/yr. The authors assumed that this difference is a result of the tectonic force acting from the south, so the calculated value of the displacement vector resulted from the tectonic push is about 0.2 mm/yr based on the aforementioned formulas.

The authors are cautious in estimating the value of the tectonic component in the displacement process. From previous research this was revealed to be an additional effect in the results of displacement measurements by a sonic probe extensometer, and the presented modeling allows an explanation of the displacement characteristics.

CONCLUSIONS

The geodetic measurements of the side walls, ceilings, and floor points; the extensometric displacement measurements; the numerical modeling of the theoretical displacements are discussed in the paper which addresses recent tectonic activity in the front of Carpathians. The investigations have been carried out in an underground environment free of the seasonal changes induced by atmospheric factors on the ground, a common problem in geodetic measurements (Szczerbowski 2009). Additionally, the observations of the displacements have been performed on intact rocks, which are penetrated by boreholes with measurement devices. The boreholes, equipped with magnetic rings, represent measurement points spread along three profiles. The displacements are oriented towards to the gallery center. This is the result of a physical process: the creation of an empty space in the plastic medium, namely rock salt, entails a compressive stress field that is proportional to the size of the void. The manifestation of the acting forces is then illustrated in the process of closure, which is manifested in the displacement of the walls. Then an outline of geometrical deformations is created and the describing deformation parameters are: the horizontal and the vertical displacements, an adequate convergence (horizontal or vertical), and the strains. The results show an asymmetric distribution of displacement rates on the opposite sides of the gallery: the northern and the southern side walls. This is completely incomprehensible when viewed solely in terms of the influence of the mining. It might be explained in terms of additional non-mining forces pushing the rock mass

particles northwards. This phenomenon can only be explained as being the result of a tectonic push of the Carpathian orogeny still shaping the Miocene salt deposit in front of it.

However, the discussed characteristic of deformation concerns the relative displacements of side walls; this is the first work in which the results show the diversity in the convergence process between the opposite sides of the baselines. They reflect the process of the displacements ongoing in the intact rocks as a result of the stress regime and the shrinking process of the gallery and this can be extrapolated for the characteristic of convergence of the longitudinal baselines in the Saint Kinga's Chapel which is located nearby. The convergence of sidewalls (whose rate is about 7–8 mm/yr) and the relative displacements of the mass particles of the inside rock surrounding the excavation, can be caused by two main effects. The first is additional stress which always exists around excavation and the second is additional geodynamic forces.

REFERENCES

Andreyeva-Grigorovich A.S., Oszczypko N., Savitskaya N., Ślączka A. & Trofimovich N., 2003. Correlation of Late Badenian salts of the Wieliczka, Bochnia and Kalush Areas (Polish and Ukrainian Carpathian Foredeep). *Annales Societatis Geologorum Poloniae*, 73(2), 67–89.

Burliga S., Krzywiec P., Dąbroś K., Przybyło J., Włodarczyk E., Źróbek M. & Słotwiński M., 2018. Salt tectonics in front of the Outer Carpathian thrust wedge in the Wieliczka area (S Poland) and its exposure in the underground salt mine. *Geology, Geophysics and Environment*, 44(1), 71–90. https:/doi.org/10.7494/geol.2018.44.1.71.

Bieniasz J. & Wojnar W., 2007. Zarys historii pomiarów i wybrane wyniki obserwacji zjawiska konwergencji wyrobisk w pokładowych złożach soli. *Gospodarka Surowcami Mineralnymi*, 23, z. spec. 1, 133–142.

Cała M., Czaja P., Flisiak D. & Kowalski M., 2009. Ocena zagrożenia zapadliskowego wybranych komór KS Wieliczka w oparciu o obliczenia numeryczne. *Górnictwo i Geoinżynieria*, 33(3/1), 33–44.

Chmura J. & Lasoń A., 2005. Projekt zabezpieczenia komory „Ważyn". *Górnictwo i Geoinżynieria*, 29(3/1), 101–117.

d'Obyrn K., J. Hydzik-Wiśniewska, 2013. Selected aspects of numerical modelling of the salt rock mass: the case of the Wieliczka salt mine. *Archives of Mining Science*, 58(1) 73–88. https:/doi.org/10.2478/amsc-2013-0005.

d'Obyrn K., Malinowska A. & Hejmanowski R., 2013. Determining mining excavations predisposed to the discontinuous deformation of land surface using a two-stage method. [in:] *XV International ISM Congress 2013 (International Society for Mine Surveying); Energie und Rohstoffe 2013 ifm & DMV: Eurogress Aachen in conjunction with the German Mine Surveyor Association (Deutscher Markscheder-Verein e.V. – DMV): September 16–20, Aachen: proceedings volumes, 1 and 2*, 592–599.

Garlicki A., 2013. Kopalnie soli na świecie [Salt mines in the world]. [in:] Nowakowski A. et al., *Skarb: Kopalnia Soli „Wieliczka" = The Wieliczka Salt Mine: an underground treasure*, Towarzystwo Autorów i Wydawców Prac Naukowych Universitas, Kraków, 15–34.

Garlicki A., 2008. Salt mines at Bochnia and Wieliczka. *Przegląd Geologczny*, 56(8/1), 663–669.

Jeremic M.L., 1994. *Rock Mechanics in Salt Mining*. CRC Press.

Knauss K.G. & Steinborn T.L., 1980. *Review of geochemical measurement techniques for a nuclear waste repository in bedded salt*. Technical Raport, Lawrence Livermore National Lab. (LLNL), Livermore, CA (United States). https://doi.org/10.2172/5474734.

Kortas G. red., 2004. *Ruch górotworu i powierzchni w otoczeniu zabytkowych kopalń soli* [*Rock mass movement in the surrounding of monument salt mines*]. Wydawnictwo IGSMiE PAN, Kraków.

Kratzsch I.H., 1986. Mining subsidence engineering. *Environmental Geology and Water Sciences*, 8, 133–136. https://doi.org/10.1007/BF02509900.

Malinowska A., Hejmanowski R., Guzy A., Kwinta A. & Ulmaniec P., 2019. The sinkhole occurrence risk mitigation in urban areas for the historic salt mine. *Environmental Science and Sustainable Development*, 4(2), 85–94. https://doi.org/10.21625/essd.v4i2.558.

Małkowski P., Bednarek Ł., Kotwica K. & Stopka G., 2019. The effect of temperature on the mechanical properties and workability of rock salt. *New Trends in Production Engineering*, 2(1), 384–393. https://doi.org/10.2478/ntpe-2019-0041.

Poborski J., 1952. *Złoże solne Bochni na tle geologicznym okolicy*. Biuletyn – Państwowy Instytut Geologiczny, 78, Wydawnictwo Państwowego Instytutu Geologicznego, Warszawa.

Poborski J., 1982. Wprowadzenie geologiczne do zagadnienia zagrożeń geodynamicznych w kopalni soli w Wieliczce. *Studia i Materiały do Dziejów Żup Solnych w Polsce*, 11, 17–28.

Puławska A., Manecki M. & Flasza M., 2021a. Mineralogical and chemical tracing of dust variation in an underground historic salt mine. *Minerals*, 11(7), 686. https://doi.org/10.3390/min11070686.

Puławska A., Manecki M., Flasza M., Waluś E. & Wojtowicz K., 2021b. Rare occurrence of mirabilite in the thirteenth-century historic salt mine in Bochnia (Poland): Characterisation, preservation, and geotourism. *Geoheritage*, 13, 36. https://doi.org/10.1007/s12371-021-00562-y.

Stoeckl L., Banks V., Shekhunova S. & Yakovlev Y., 2020. The hydrogeological situation after salt-mine collapses at Solotvyno, Ukraine. *Journal of Hydrology: Regional Studies*, 30, 100701. https://doi.org/10.1016/j.ejrh.2020.100701.

Szczerbowski Z., 2009. Toward the reliability of geodetic surveys in study of geodynamics – a problem of influence of seasonal variations. *Acta Geodynamica et Geomaterialia*, 6(3), 253–263.

Szczerbowski Z., 2020. Irregularity of post mining deformations as indicator revealing effects of processes of unknown origin in area of Bochnia. *Geoinformatica Polonica*, 19, 81–93. https://doi.org/10.4467/21995923gp.20.008.13073.

Szczerbowski Z. & Niedbalski Z., 2021. The application of a sonic probe extensometer for the detection of rock salt flow field in underground convergence monitoring. *Sensors*, 21(16), 5562, 1–17. https://doi.org/10.3390/s21165562.

Szczerbowski Z., Kaczorowski M., Wiewiórka J., Jóźwik M., Zdunek R. & Kawalec A., 2016. Monitoring of tectonically active area of Bochnia. *Acta Geodynamica et Geomaterialia*, 13(1), 59–67. https://doi.org/10.13168/AGG.2015.0044.

Szostak-Chrzanowski A., Chrzanowski A. & Massiéra M., 2005. Use of deformation monitoring results in solving geomechanical problems – case studies. *Engineering Geology*, 79(1–2), 3–12. https://doi.org/10.1016/j.enggeo.2004.10.014.

Szwedzicki T., 2018. *Rock Mass Response to Mining Activities: Inferring Large-Scale Rock Mass Failure*. CRC Press.

Toboła T. & Bezkorowajny A., 2006. Przejawy ruchów neotektonicznych i współczesnych w bocheńskiej kopalni soli kamiennej [Neotectonic and recent movements revealed in the Bochnia salt mine]. *Geologia: kwartalnik Akademii Górniczo-Hutniczej im. Stanisława Staszica w Krakowie*, 32(1), 5–19.

Wiewiórka J., Charkot J., Dudek K. & Gonera M., 2008. Historic salt mines in Wieliczka and Bochnia. *Geotourism/Geoturystyka*, 4(18), 61–70. https://doi.org/10.7494/geotour.2009.18.3.61.

Wiewiórka J., Dudek K., Charkot J. & Gonera M., 2009. Natural and historic heritage of the Bochnia salt mine (South Poland). *Studia Universitatis Babeş-Bolyai. Geologia*, 54(1), 43–47.